Linking drought strategy to climate of origin in a widespread C4 grass species: hydraulic traits, xylem anatomy and stomatal behaviour in *Themeda triandra*

Vinod Jacob, Chris J. Blackman, Brendan Choat, Brian Atwell, Eloise Foo, Alejandro Correa-Lozano, Travis Britton, Emma E. Sumner, Ian J. Wright

SUMMARY

- Hydraulic, stomatal and anatomical traits significantly influence drought survival and productivity, but the extent to which these traits are coordinated and align with climate of origin (COO) in herbaceous species remains poorly understood.

- We quantified hydraulic, stomatal and anatomical traits in eight populations of *Themeda triandra* selected from diverse temperature and precipitation regimes across Australia, grown under common conditions and exposed to drought. Trait-climate-of-origin relationships were quantified using multiple linear mixed models.

- Leaf xylem embolism resistance (P_{50}) was unrelated to precipitation-of-origin but plants from drier climates exhibited lower maximum stomatal conductance, earlier stomatal closure during drought and higher stomatal safety margins (the difference between water potential at stomatal closure and P_{50}). Plants from warmer climates exhibited greater embolism resistance and higher hydraulic conductance, along with wider vessels and lower vein density, suggesting adaptation to high evaporative demand rather than aridity.

- Our findings highlight two primary hydraulic strategies related to climate of origin: 1) conservative water use and drought avoidance in drier climates, and 2) drought resistance and hydraulic efficiency in warmer climates. These findings provide new insights into the intraspecific differences in traits and adaptive strategies used by C_4 grasses to persist in contrasting climates.

INTRODUCTION

Understanding the physiological and anatomical adaptations that underpin plant success in different environments is a primary goal of plant ecology and critical for predicting vegetation responses to climate change (Madani *et al.*, 2018; Bjorkman *et al.*, 2018). Hydraulic traits, which govern how plants transport and retain water, play a central role in determining plant survival and productivity (Choat *et al.*, 2012; Powers *et al.*, 2020). A key measure of how plants maintain function under transient water deficits is the water potential (-MPa) at which 50% of hydraulic conductivity is lost due to embolism, P_{50} (Maherali *et al.*, 2004; Markesteijn *et al.*, 2011; Choat *et al.*, 2018). While resistance to xylem embolism defines the lower bounds of water potential that a plant can tolerate before irreversible drought injury occurs, the likelihood of reaching this critical threshold is largely modulated by stomatal regulation (Skelton *et al.*, 2015, Martin-StPaul *et al.*, 2017). Stomata regulate water and carbon exchange by responding to soil water deficits through gradual closure, minimizing water loss and slowing further declines in xylem water potential (Tyree & Sperry, 1988; Sperry, 2000). Water potential at which 90% of stomatal conductance is lost due to stomatal closure (g_{s90}) is a commonly used variable to quantify stomatal behaviour (Brodribb & Holbrook, 2003; Martin-StPaul *et al.*, 2017). By comparing water potential thresholds of stomatal closure and xylem embolism (P_{50} and g_{s90}, respectively), a "stomatal safety margin" (SSM) can be defined where SSM = $P_{50} – g_{s90}$. Hydraulic strategies vary widely among plants, ranging from conservative (isohydric; stomata close in advance of xylem failure/high SSM) to risky (anisohydric; stomata remain open even after the onset of embolism/neutral or negative SSM) (Klein, 2014; Hochberg *et al.*, 2018; Hartmann *et al.*, 2021). In this study we examined variation in P_{50}, g_{s90} and SSM across populations of the widespread C4 grass, *T. triandra*, grown under common conditions. We tested hypothesised relationships between these key traits and climate-of-origin (COO; where seeds were sourced), investigating the anatomical basis of hydraulic trait variation, and coordination between hydraulic and photosynthetic traits.

In common-environment studies, hydraulic and stomatal traits often relate to COO, with species from drier environments typically exhibiting more negative P_{50} values, indicating greater resistance to embolism (Ocheltree *et al.*, 2016; Bourne *et al.*, 2017; Li *et al.*, 2018; Volaire *et al.*, 2018). Stomatal closure thresholds (g_{s90}) similarly tend to decline with aridity (Bourne *et al.*, 2017; Li *et al.*, 2018) such that species or poulations from drier sites close stomata at less negative water potentials. Leaf turgor loss point (the water potential at which leaves begin to wilt; Ψ_{TLP}), tends also to be more negative in dry-adapted taxa; indeed Ψ_{TLP} is widely used as a proxy for drought tolerance (Bartlett *et al.*, 2014; Maréchaux *et al.*, 2015; Bourne *et al.*, 2017; Blackman, 2018). However,

relationships between hydraulic traits and site temperature are less well studied and show inconsistent patterns, with a large meta-analysis reporting negative associations between temperature and P_{50} (Nardini & Luglio, 2014), but others studies have found both positive (Hartill *et al.*, 2023; Huang *et al.*, 2024) or no relationship (Li *et al.*, 2018; López *et al.*, 2021). Li *et al*. (2018) also reported no relationship between site temperature and g_{s90}. The relationship between P_{50} and temperature is likely influenced by both the risk of freeze-thaw embolism in cold climates (Davis *et al.*, 1999; Pittermann & Sperry, 2006) and the risk of water-stress-driven embolism in hot, dry climates.

Xylem anatomical traits underpin key hydraulic properties, however their role in modulating hydraulic conductivity and embolism resistance in species across environmental gradients remains poorly understood. Hydraulic conductivity increases with conduit diameter to the fourth power (Sperry et al., 2006), but wider vessels may be more vulnerable to embolism, depending on the interaction between vessel size and pit membrane thickness (Choat *et al.*, 2008; Lens *et al.*, 2022). Wide vessels are advantageous in warm environments, where high evaporative demand necessitates efficient water transport (Morris *et al.*, 2018; Olson *et al.*, 2018; Fontes *et al.*, 2022), but disadvantageous in dry environments, where the risk of drought-induced embolism increases (Olson *et al.*, 2018; Fontes *et al.*, 2022). Accordingly, plants from drier climates tend to have narrower vessels that are more densely packed (i.e. more vessel units per cross-sectional area), likely in order to compensate for reduced vessel size (Pfautsch *et al.*, 2016), facilitating the maintenance of overall conductivity through redundancy without sacrificing embolism resistance (Zanne *et al.*, 2010; Bayramzadeh *et al.*, 2011; Fontes *et al.*, 2022; Zhang *et al.*, 2024). Vessel wall thickness is also closely linked to embolism resistance (Lens *et al.*, 2016; Li *et al.*, 2016; Volaire *et al.*, 2018), possibly via thicker pit membranes (Li et al., 2016; Thonglim et al., 2021), and may also function as an adaptation to freeze-thaw embolism in cooler climates (Davis *et al.*, 1999; Choat *et al.*, 2011; Echeverría *et al.*, 2022; Huang *et al.*, 2024).

Much of our current understanding of plant hydraulic traits and their anatomical determinants comes from studies of woody species (Blackman *et al.*, 2014; Skelton *et al.*, 2015; Bourne *et al.*, 2017; López *et al.*, 2021). By contrast, hydraulic traits in herbaceouse plants remain comparatively understudied, and their relationships with climate are poorly resolved (Griffin-Nolan *et al.*, 2018; Griffin-Nolan & Sandel, 2023). Furthermore, while hydraulic traits have been well described across broad taxonomic scales (Choat *et al.*, 2012; Nardini and Luglio, 2014; Huang *et al.*, 2024), within-species variation is less well understood (Wortemann *et al.*, 2011; López *et al.*, 2021). Grasses dominate over 40% of the Earth's terrestrial surface and are crucial for global agriculture

(McSteen & Kellogg, 2022) but studies of within-species variation in the relationship between xylem embolism and stomatal regulation in grasses and how this variation is driven by site climate is lacking.

The ability of woody species to survive intense drought is strongly related to xylem vulnerability to embolism (McDowell *et al.*, 2008; Choat *et al.*, 2018). However, the traits and processes involved in the survival and recovery of grass species after extreme drought are often more complex and multifaceted (Craine *et al.*, 2013; Hoover *et al.*, 2014). Like woody species, perennial grasses from arid environments may exhibit drought tolerance (embolism resistance) or drought avoidance (early loss of turgor and stomatal closure) strategies but can also employ alternative mechanisms such as aboveground senescence and/or dormancy to survive drought (Volaire *et al.*, 2009; Zwicke *et al.*, 2015; Balachowski *et al.*, 2016; Keep *et al.*, 2021). *T. triandra Forssk*. is a perennial C4 tussock grass in the Andropogoneae tribe (which includes major crops like sorghum, maize, and sugarcane) and is the most widespread plant species in Australia (Gallagher, 2016) thriving across all biomes from semi-arid savannas and seasonally wet tropics to sub-alpine and cool temperate regions (Hayman, 1960; Dunning et al., 2017, 2022). The exceptional climatic breadth and ecological dominance of this species makes it ideal for examining how grasses have evolved diverse strategies to cope with drought and to investigate how hydraulic and other physiological traits are driven by climate adaptation more broadly.

In this study we quantified the xylem embolism resistance, stomatal regulation, and other key hydraulic and anatomical traits in eight accessions of *T. triandra* collected from sites with diverse temperature and rainfall (defined here as the climate-of-origin; COO). We tested whether trait–trait relationships related to the proposed hydraulic safety–efficiency trade-off (Hacke *et al.*, 2006; Gleason *et al.*, 2016; Ocheltree *et al.*, 2016) and if other key hydraulic–anatomical associations (Hacke *et al.*, 2001; Sperry *et al.*, 2006; Chen *et al.*, 2020) hold within this species. By simultaneously investigating hydraulic, anatomical, and gas exchange traits across multiple *T. triandra* populations grown in a common garden, this study reveals the functional strategies that enable persistence across diverse climates and enables the disentangling of genetic variation from environmentally-induced plasticity (Jankowski *et al.*, 2019; Huxman *et al.*, 2022; Schwinning *et al.*, 2022). Understanding these within-species patterns in a wild Andropogoneae grass may provide insights for predicting shifts in native grassland composition under climate change, and provides useful context for enhancing drought resilience in related crop species.

Our work tested a number of hypotheses based on fundamental principles of plant hydraulics, and previous empirical trends reported in the literature:

126 **Hypotheses**

127 1. Plants from drier environments would exhibit more negative values for P_{50}, Ψ_{TLP}, and g_{s90} and
128 have smaller, thicker-walled vessels with higher density, limiting water loss and reducing
129 embolism risk.
130 2. Plants from warmer sites would exhibit higher hydraulic conductance (K_{leaf}), facilitated by wider
131 vessels, enabling more efficient water transport and sustained leaf function under high
132 evaporative demand.
133 3. Plants with more negative P_{50} would have smaller vessels and thicker xylem vessel walls
134 accompanied by lower K_{leaf}, in accordance with an assumed hydraulic safety-efficiency trade-off.

135 In addition, we expected traits related to rapid resource capture (A_{max}, K_{leaf}, and g_{smax}) to covary
136 positively among themselves but negatively with traits related to stress tolerance (P_{50}, Ψ_{TLP}, and g_{s90}),
137 reflecting a trade-off between distinct adaptive strategies.

138

139 Methods

140 **Plant Growth**

141 We grew 10–12 replicates of eight populations of *T. triandra*, sourced from diverse climatic regions
142 across Australia (Figure 1, Table S2; summer temperatures ranging from 16.3 – 32.1°C and summer
143 precipitation ranging from 75 - 435 mm), in a climate-controlled glasshouse at the Hawkesbury
144 Institute for the Environment, Western Sydney University, Richmond, NSW. Plants were grown from
145 seeds germinated in seed trays. After emergence they were transplanted into 8 litre pots filled with
146 sandy-loam soil (pH ≈ 5.6) collected from the PACE field facility at Western Sydney University
147 (Churchill *et al.*, 2022). The soil in each pot was supplemented with 10 g of slow-release native-plant
148 fertiliser (Osmocote® Native). Seedlings subsequently received a half-strength application of Yates
149 Thrive® All-Purpose fertiliser (N:P:K 25:5:8), applied weekly for the first four weeks, to prevent
150 nutrient limitation during establishment.

151 All pots were maintained at 100% field capacity, using an automated irrigation system, for the first
152 two months of growth. The glasshouse was maintained at 30/20°C (day/night) temperatures with
153 ambient CO_2 levels (~420 ppm) and a 14-h light period. Natural light was supplemented throughout
154 the light period with full spectrum LED lighting, adding 700 µmol photons m^{-2} s^{-1}, with maximum
155 midday levels reaching ~1500 µmol photons m^{-2} s^{-1}. Following this initial growth period, all plants

underwent a “drought-hardening” pre-treatment, in which watering was withheld for 4–5 days, inducing visible leaf wilting. After this period of water deficit, plants were rewatered to 100% field capacity and maintained under these conditions for 4–6 days, ensuring full rehydration (predawn leaf water potential ≈ 0). All plants were maintained at 100% field capacity for an additional two weeks before being allocated to two experimental groups: 1) “Steady-State Trait Characterisation” plants were used to measure key hydraulic, physiological and anatomical traits, and 2) “Dynamic Dry-Down Assay” plants were subjected to a progressive dry-down to assess stomatal responses to desiccation.

Steady-State Trait Characterisation

Leaf xylem vulnerability measurements

The optical vulnerability (OV) technique (Brodribb *et al.*, 2016) was used to visualise embolism events and estimate vulnerability thresholds in the leaves of 4-5 replicates for each population. Whole individual plants (including root systems) were carefully removed from pots early in the morning and roots were washed to remove any soil. Excised plants were placed in a bucket containing a shallow layer of water and covered with black plastic bags to ensure that they remained well hydrated, so embolism due to dehydration did not occur before OV measurements began. Plants were transported immediately to the laboratory for OV measurements, where a fully expanded leaf from each individual was positioned between two plastic polarising films and placed into a CaviCam clamp. The Cavicam consists of a Raspberry Pi single board computer (Raspberry Pi Foundation, http://www.raspberrypi.org) which controls and stores images produced by an 8-Mp camera magnified by a ×20 lens. Leaf samples were illuminated from below using six light-emitting diodes (LEDs) delivering ~200 µmol quanta m^{-2} s^{-1} to the leaf and providing refracted light from the sample surface to the camera. All components were housed within a 3D-printed clamp (further details of the clamps are provided at https://github.com/OpenSourceOV).

Leaf water potential was concurrently measured on the nearest neighbouring leaf using a stem psychrometer (ICT PSY Armidale, NSW, Australia) (Johnson *et al.*, 2018). The psychrometer was automated to take water potential readings every 10 minutes, and the accuracy of the psychrometer was verified for a subset of individuals using a Scholander pressure chamber (PMS Instruments) (Figure S2); leaves of similar size were used for all individuals for consistency. Both water potential and xylem images were recorded until each plant had dehydrated completely (i.e. embolism events had ceased for >12 hours).

Images of xylem embolism were processed using ImageJ using the instructions at https://github.com/OpenSourceOV/image-processing-instructions/blob/master/instructions.md. Differences between neighbouring images in each sequence were used to highlight embolism events. Rapid changes in pixel intensity associated with embolism are distinguishable from other changes in the leaf during dehydration (Johnson *et al*. 2018). Threshold analyses were used to remove noise related to leaf movement, in order to produce a set of images that contain only the pixels associated with embolism events. These data were used to determine the percentage of embolism using the following equation.

$$\%embolism = \frac{A_{emb}}{A_{total}} \times 100,$$

Where A_{emb} is the cumulative area of embolised xylem at a given time and A_{total} is the total area of embolised xylem at the end of sample dehydration. Finally, the water potential data were combined with the total cumulative pixel count to create a vulnerability curve for each species.

Maximum rates of leaf gas exchange and leaf hydraulic conductance

Steady state measurements of net photosynthesis (A_{sat}; µmol m^{-2} s^{-1}), stomatal conductance (g_s; mol m^{-2} s^{-1}) and transpiration (*E*; mmol m^{-2} s^{-1}) were conducted on 4-5 replicates of each population between 09:00 and 12:00 on recently fully expanded leaves using a portable open, infra-red gas exchange system (LI-6800, Li-Cor, Lincoln, NE, USA). Measurements were conducted at a saturating photosynthetic photon-flux density (PPFD) of 1800 mmol m^{-2} s^{-1} and a chamber reference [CO_2] (C_a) of 420 µmol CO_2 mol^{-1} at average daily mid-day temperatures (30 °C). Leaf-to-air vapour pressure deficit levels were maintained at roughly 1.5–2.0 kPa. Each leaf was allowed ~5 mins to equilibrate before measurements were taken (Ghannoum *et al*. 2010). Well-watered control pots from experiment 2 were also measured daily until the end of the experiment and A_{sat} and g_s values were averaged across multiple timepoint to calculate g_{smax} and A_{max}.

Maximum leaf hydraulic conductance (K_{leaf}) was measured using the "relaxation by rehydration" method (Brodribb & Holbrook, 2003). A pair of adjacent leaves were selected based on similar size and condition from well-watered individuals (either two leaves from the same tiller or adjacent leaves). The initial leaf water potential (Ψ_0) was measured on the first leaf, using a pressure chamber, and the second leaf was partially submerged in filtered, de-ionized water, and recut at the base and rehydrated for 30 seconds. The apical section of the leaf remained out of the water, ensuring that rehydration occurred only through the cut xylem. After rehydration, the second leaf

218 was re-cut above the water line and placed in a pressure chamber to obtain the final rehydrated leaf
219 water potential (Ψ_f). Leaf hydraulic conductivity (K_{leaf}) was calculated using the following equation.

220 $$K_{leaf} = \frac{C_{leaf} \ln\left(\left[\frac{\Psi_0}{\Psi_f}\right]\right)}{t}$$

221 where C_{leaf} is the bulk leaf capacitance before turgor loss, normalized by leaf area, t is the duration of
222 rehydration, and Ψ_0 and Ψ_f are the initial and final leaf water potentials, respectively.

223 *Pressure Volume Curves*

224 Pressure volume curves were conducted on multiple leaves from 4-5 individuals from each
225 population to determine turgor loss point (ΨTLP) and C_{leaf}. Leaves were sampled at dusk and placed
226 in opaque plastic bags, with the distal end of each leaf placed under water, and left to rehydrate
227 overnight. Rehydrated leaves were photographed, and images were analysed using imageJ to
228 calculate leaf area. Leaf fresh weight (FW) and Ψ_{leaf} were then periodically measured during slow
229 desiccation, until Ψ_{leaf} reached -3 MPa. Sample leaves were then oven dried at 70 °C for a minimum
230 of 48 hr to obtain dry weight (DW). Ψ_{TLP} was calculated by plotting leaf relative water content
231 (RWCleaf, %) against the inverse of Ψ_{leaf} , and Ψ_{TLP} was determined as the point where the line
232 became non-linear. Area-based leaf-specific capacity at full turgor (C_{leaf}) and leaf osmotic potential at
233 full turgor (Ψosm) were calculated for each individual leaf following standard pressure-volume curve
234 analysis methods (Turner, 1988; Sack et al., 2011) and averaged across replicate leaves of the same
235 plant.

236 *Analyses of xylem characters using light microscopy*

237 Leaf samples from the same individuals used for leaf hydraulic vulnerability measurements were
238 collected and immediately fixed in a 5% formaldehyde, 5% acetic acid, and 70% ethanol solution (FAA)
239 solution for 48 hours to preserve tissue structure. Following fixation, samples were gradually
240 dehydrated through an ethanol series up to 70% for long-term storage before embedding. Fixed
241 samples were embedded in Optimal Cutting Temperature compound (Tissue-Tek® O.C.T. Compound,
242 Sakura Finetek, USA) and sectioned at -25°C and 6 µm thickness using a cryostat (HM525 NX, Epredia).
243 Sections were transferred by gentle pressure contact onto 1.3% Fol's chrom-alum gelatine subbed
244 glass slides (Kiernan, 1999). For staining, sections on slides were first submerged in 1% Safranin O for
245 10 minutes, to stain lignified tissues. Samples were then dehydrated in 70% ethanol and
246 counterstaining was performed with 0.5% Fast Green (in absolute ethanol). Finally, sections were

247 cleared in xylene and dry specimens were mounted permanently with Eukitt mounting medium
248 (Sigma-Aldrich).

249 Images from each population were captured using an Axiocam 503 color module (Zeiss) attached to
250 an Axioscope 5 (Zeiss) microscope under a phase contrast setup. Leaf anatomical traits were
251 quantified via image analysis using Fiji, ImageJ2 (ImageJ v. 1.54f). Measured traits included vein
252 density and diameter for both major and minor veins, and metaxylem vessel wall thickness for major
253 veins. For each replicate, two measurements were taken and the mean reported. Vein diameter was
254 quantified as the tangential diameter of the two largest vessels, measured at the widest point of the
255 lumen (excluding cell walls), and expressed as arithmetic means. Vessel wall thickness was measured
256 on metaxylem vessels in major veins. Vein density was determined by counting individual major and
257 minor veins per leaf section and normalizing by leaf section length (veins cm^{-1}), determined using a
258 white reference line along the blade margin. Further methodological details, measurement protocols
259 and representative images, are provided in Table S4.

260

261 *Dynamic Dry-Down Assay*

262 One replicate pot from each population was maintained at 100% field capacity to serve as the well-
263 watered control while four other replicates of each population were subjected to a prolonged,
264 severe dry-down by completely withholding irrigation. Soil moisture was measured daily using a
265 handheld soil water reflectometer (HydroSense II CS659, Campbell Scientific). Predawn (Ψ_{PD}) and
266 midday (Ψ_{MD}) leaf water potentials were also measured daily, using a Scholander pressure bomb
267 (PMS Instruments, Albany, OR, USA) fitted with a grass compression gland and base, on two to three
268 leaves per individual to track plant water status. Concurrently, daily measurements of light-
269 saturated photosynthesis (A*sat*; µmol m^{-2} s^{-1}), stomatal conductance (g_s; mol m^{-2} s^{-1}), transpiration
270 (*E*; mmol m^{-2} s^{-1}) and chlorophyll fluorescence (F_v/F_m)—were taken on the same leaves. These data
271 were used to derive the leaf water potential at 90 % stomatal closure (g_{s90}). Steady state
272 measurements of A_{sat}, g_s and *E* were conducted between 09:00 and 12:00 on recently fully expanded
273 leaves using the LI-6800 (described above). Measurements were conducted at a saturating PPFD of
274 1800 mmol m^{-2} s^{-1} with a chamber reference [CO_2] (C_a) of 420 µmol CO_2 mol^{-1} and at average daily
275 mid-day temperatures (30 °C). Leaf-to-air vapour pressure deficit levels were maintained at roughly
276 1.5–2.0 kPa. Each leaf was allowed ~5 mins to equilibrate before measurements were taken.
277 Measurements were conducted daily on the dehydrating pots (on 2-3 leaves from each individual

plant per day) until stomatal closure occurred (i.e. g_s was reduced by > 90%). All parameters were also measured on well-watered control pots until the end of the experiment.

Climate data

As described in the Introduction, *T. triandra* occurs across a variety of climate zones in Australia (Dunning *et al.*, 2017; Arthan *et al.*, 2022). To identify the most appropriate climate-of-origin descriptors for this comparative study, ten climatic variables capturing temperature and precipitation means, seasonality, and extremes for each of the eight source locations were extracted from CHELSA gridded datasets (Karger *et al.*, 2017), which report long-term (1981 – 2010) interpolated climate averages at a spatial resolution of ~ 1km at the equator. Principal components analysis was used to identify the major tendencies across these ten variables, with varimax rotation applied to improve interpretability (by aligning climate vectors more clearly with individual factors rather than composite mixtures). The first rotated axis reflected a temperature–seasonality gradient (driven by temperature range and mean summer temperature). The second axis captured a precipitation gradient (driven by summer and annual precipitation). From these analyses we selected *summer temperature* and *summer precipitation* as the key climate variables to be used in analysis of trait – climate relations. These two variables had the strongest loadings (Table S3) on their respective axes and have clear biological relevance given, although perennial, this species exhibits peak growth during the warmer summer months, especially in colder regions where its growth is restricted to this period (Snyman *et al.*, 2013; Churchill *et al.*, 2022; Male *et al.*, 2022). These variables were largely independent (R^2 = 0.03, P = 0.698), allowing their use in subsequent models. Note, we used statistical approaches (described below) that simultaneously considered the effects of two climate variables, allowing us to quantify trait relationships with summer temperature *with variation in summer rainfall held constant*, and vice versa.

Statistical Analysis

Leaf hydraulic vulnerability curves were fitted using the "fitplc" function from the "fitplc" package (Duursma & Choat, 2017), using Weibull models where they converged and sigmoidal models when curves exhibited abrupt, steep declines in conductance that caused non-linear optimisation to break down. Individual vulnerability curves were generated for each replicate plant and the leaf water potentials causing 12% (P_{12}) and 50% (P_{50}) xylem embolism were quantified. Stomatal conductance values were plotted against leaf water potential and fitted with a weighted polynomial regression, using the "*fitcond*" function within the "*fitplc*" package, to extract leaf water potential at stomatal

closure (g_{s90}). Stomatal safety margins (MPa) were calculated as the difference between the Ψ_{MD} at which stomata were 90% closed (gs_{90}) and P_{50} (SSM).

To assess the relationship between plant functional traits and the two climate variables, we used linear mixed-effects models fitted with the "lme4" package in R. The model structure included a response variable (trait of interest) as a function of climate predictors. To incorporate the repeated sampling structure of the data, the site of origin for each population was specified as a random effect:

$$model = trait \sim Summer\ Precip + Summer\ Temp + (1|Accession)$$

A corresponding fixed-effects linear model was also fit without the random effect for visualization of partial residuals. We also tested for an interaction between summer precipitation and summer temperature for each trait but found no significant interactions, so we retained an additive model structure. The effect of each climate predictor on the response trait was visualized using the "visreg" package, extracting model residuals to generate partial residual plots. This approach allows for the visualization of the independent effects of precipitation and temperature on the trait of interest while accounting for the influence of other variables in the model. P-values for fixed effects were quantified using the "lmerTest" package.

To assess the robustness of our findings, we also conducted bivariate analyses of each climate variable independently. This approach allowed us to examine whether incorporating both precipitation and temperature in the mixed model influenced our results by accounting for covariation between these climate factors. Additionally, bivariate analysis strengthens our results by providing a complementary perspective on trait-climate relationships, helping us determine which correlations remain consistent across different analytical approaches. Moreover, we included a annual moisture index (calculated as precipitation/potential evapotranspiration) in our bivariate analysis, this being a widely used, an integrated measure of site water availability.

Results

We observed marked variation in the various hydraulic safety and efficiency traits in *T.triandra* populations from different climates. Population-mean xylem embolism resistance (P_{50}) ranged from –2.41 MPa in plants from Hobart (southern Australia) to –5.13 MPa in plants from Pannawonica (north-western Australia). Traits governing plant water status showed less variation, with

339 population-mean turgor loss point (Ψ_{TLP}) varying between –1.17 and –1.86 MPa and the threshold
340 for near-complete stomatal closure (gs_{90}) ranging from –3.93 to –5.44 MPa. Consequently, stomatal
341 safety margins (SSM = $P_{50} – g_{s90}$) spanned from positive values (+0.75 MPa) to negative values (–1.54
342 MPa. This indicates that in populations with a positive SSM, total stomatal closure preceded the
343 onset of embolism (Rainbow Valley, Virginia, Pannawonica and Forbes), whereas in those with
344 negative SSM it lagged behind (Mt Fox National Park, Hobart, Dalby and Sydney). Leaf hydraulic
345 conductance (K_{leaf}) varied markedly, from 2.53 to 11.10 mmol m^{-2} s^{-1} MPa^{-1}, indicating substantial
346 differences in hydraulic efficiency between populations.

347

348 ***Climate-related trends in hydraulic traits***

349 We predicted (Hypothesis 1) that populations from drier sites would display more negative P_{50}, Ψ_{TLP}
350 and g_{s90} values than those from wetter sites; i.e., drier site plants to be more resilient to water
351 stress. Instead, in linear mixed models (LMMs) including both summer precipitation and summer
352 temperature as predictors, P_{50} and precipitation were unrelated (Fig. 2A), while dry-site populations
353 exhibited *less* negative Ψ_{TLP} (Fig. 2C) and earlier stomatal closure than wetter sites (less negative g_{s90};
354 Fig. 2E). This was also the case in the bivariate trait–precipitation analyses (Table S1). Dry-site
355 populations exhibited a coordinated suite of drought-avoidance traits rather than the expected suite
356 of drought resilience traits. Their stomatal safety margins (SSM; calculated as $P_{50} – g_{s90}$) were higher
357 (~0 or weakly positive,) than observed in plants from wetter sites, indicating that these plants closed
358 their stomata before the onset of xylem embolism (Fig. 2G). This trend was driven by g_{s90} rather than
359 P_{50}. K_{leaf} was significantly higher in populations from drier sites than in wetter sites(Fig. 2I). Neither of
360 the SSM or Kleaf trends were observed in bivariate analyses (Table S1).

361 Using LMM analysis, populations originating from warmer climates exhibited greater drought
362 tolerance, as indexed by more negative P_{50} (Fig. 2B). However, Ψ_{TLP} (Fig. 2D) and g_{s90} (Fig. 2F) were
363 unrelated to site temperature. These tendencies were also observed in bivariate trait–temperature
364 analyses (Table S1). The positive relationship between temperature and P_{50} indicated a tendency for
365 plants from warmer climates to exhibit higher SSMs than plants from cooler climates (Fig. 2H),
366 although this was observed in the LMM analysis only. In support of Hypothesis 2, warm-origin plants
367 had significantly higher K_{leaf} than cool-climate plants (Fig. 2J) in the LMM if analysis only (Table S1).

368 Moisture Index (the annual balance between precipitation and potential evapotranspiration) at the
369 climate of origin had little effect on hydraulic traits except that plants from more arid environments
370 exhibited marginally higher hydraulic conductance than those from mesic sites (P = 0.067; Table S1).

371 ***Climate-related trends in xylem anatomy***

372 Neither major nor minor vessel diameter varied with precipitation, whether considered
373 simiultaneoulsy with temperature variation (LMMs: Figs 3A,E) or in bivariate analyses (Table S1). This
374 was counter to our expectation of narrower vessels at drier sites (Hypothesis 3). We also expected
375 dry-origin plants to display thicker vessel walls, but observed no relationship between vessel wall
376 thickness and precipitation (Fig. 3, I,J). Vessel density (number per cross-sectional area) was also
377 unrelated to precipitation (Fig. 3C,G; Table S1).

378 Relationships to site temperature differed between vein types: major vein traits were unrelated to
379 temperature (Fig. 3B,D; Table S1), whereas minor vein traits showed distinct temperature-driven
380 trends. Plants from hotter sites had wider minor vein vessels (Fig. 3F) and reduced minor vein
381 density compared to cooler sites (Fig. 3H). The same trends were also evident in bivariate trait–
382 climate analyses (Table S1). Moisture Index was not correlated with vessel diameter (both minor and
383 major veins) but plants from more arid sites had lower minor vein density than those from more
384 mesic sites (P = 0.049 Table S1).

385

386 ***Photosynthetic traits and climate***

387 In LMMs, A_{max} was not significantly related to climate-of-origin (Fig. 4A, B), however, g_{smax} was
388 significantly higher in plants from wetter environments (Fig. 4C) and marginally higher in plants from
389 colder sites (Fig 4D). These relationships were consistent in bivariate trait-climate analyses (Table
390 S1).

391

392 **Coordination among hydraulic, anatomical and photosynthetic traits**

393 We found no evidence of the expected trade-off (Hypothesis 3) between hydraulic safety, as indexed
394 by P_{50} and g_{s90}, and hydraulic efficiency, either as indexed by K_{leaf} (Fig. 5A,D) or g_{smax} (Fig. 5B, E).
395 Variation in P_{50} was also unrelated to A_{max} and g_{smax} (Fig. 5C,D). By contrast, populations that lost
396 turgor at less negative water potentials (i.e. had less negative Ψ_{TLP}) typically had lower g_{smax} (R^2 =
397 0.55, P < 0.036; Fig. 5H) and A_{max} (R^2 = 0.45, P = 0.067; Fig. 5I).

398 Contrary to expectations, plants that were more resistant to embolism (more negative P_{50}) had
399 wider major vein vessels (R^2 = 0.61, P = 0.023; Fig. 6A) and wider minor vein vessels (R^2 = 0.52, P =
400 0.043; Fig. 6C). Plants with more negative P_{50} also had fewer minor veins density (R^2 = 0.48, *P* =
401 0.056; Fig. 6D), but there was no relationship with major vein density (Fig. 6B). Against expectations,

402 major vein vessel wall thickness was unrelated to P_{50} (Fig. 6E). Variation in hydraulic conductivity
403 (K_{leaf}) was largely unrelated to xylem anatomy, except that plants with lower density of minor veins
404 had higher K_{leaf} ($R^2 = 0.79$, $P = 0.003$; Fig. 6I). K_{leaf} was not correlated with major vessel vein vessel
405 diameter (Fig. 6F) or major vein density (Fig. 6G).

406 We found no evidence of coordination between xylem embolism resistance (P_{12} & P_{50}) and stomatal
407 closure (g_{s90}; Fig. 7A, C, E) or turgor loss point (Ψ_{TLP}; Fig. 7B, D). However, Ψ_{TLP} exhibited a positive
408 relationship with g_{s90} (Fig. 7E), as we found that plants that lost turgor at less negative water
409 potentials also showed marked reductions in stomatal conductance at these less negative water
410 potentials. We expected to see K_{leaf} being positively correlated with leaf gas exchange traits. Instead,
411 we observed clear negative relationships between K_{leaf} and each of A_{max} (Fig. 8A) and g_{smax} (Fig. 8B).

412

413 Discussion

414 We explored the relationships between key hydraulic traits related to water-use, xylem embolism
415 resistance and stomatal regulation, as well as a range of photosynthetic and anatomical traits in
416 eight populations of *T. triandra* selected from diverse climatic regions across Australia varying
417 strongly in precipitation and temperature. Linear mixed models revealed contrasting trait syndromes
418 associated with local rainfall and temperature conditions at climate-of origin (COO). Our results
419 challenge commonly assumed trait trade-offs, suggesting a more nuanced coordination of hydraulic
420 function and gas exchange traits across populations of this widespread grass species. These findings
421 provide insight into how diverse drought tolerance strategies emerge within a single species and
422 highlight key traits that may enhance resilience under future climates.

423

424 ***Trait–Climate Interactions and Adaptive Strategies in T. triandra***

425 Our finding that leaf P_{50} was not related to precipitation did not accord with our first hypothesis or
426 numerous cross-species studies, mainly on woody species, that have reported increased embolism
427 resistance in drier environments (Nardini & Luglio, 2014; Blackman *et al.*, 2014; Ocheltree *et al.*,
428 2016; Bourne *et al.*, 2017; Li *et al.*, 2018; Volaire *et al.*, 2018; Yao *et al.*, 2021). Intraspecific studies,
429 on the other hand, often show weak or no correlation between P_{50} and precipitation (Martínez-
430 Vilalta *et al.*, 2009; Bayramzadeh *et al.*, 2011; Lamy *et al.*, 2014; Blackman *et al.*, 2017). The lack of a
431 relationship between P_{50} and precipitation we observed across populations of *T. triandra* may also
432 reflect fundamental differences in drought response and carbon allocation strategies between

433 woody plants and grasses. Woody species (especially evergreens) generally maintain the same
434 conductive tissues through successive periods of water deficit, exposing them to repeated embolism
435 risk. In contrast, grasses such as *T. triandra* can senesce above-ground organs during drought and
436 regenerate foliage via basal meristems once drought is alleviated (Volaire *et al.*, 2009; VanderWeide
437 *et al.*, 2014), reducing the need to maintain embolism-resistant tissues. This capacity for resprouting
438 may also explain the lack of relationship between leaf P_{50} and drought survival observed by
439 Ocheltree *et al.* (2016) in several other perennial grass species. Rather than selection for increased
440 leaf embolism resistance, plants from drier environments exhibited turgor loss and stomatal closure
441 at less negative water potentials than plants from wetter environments. Hence populations from the
442 drier sites maintain a positive SSM —indicating that stomata closed before embolism occurred —
443 while plants from wetter sites exhibited negative SSM, tolerating some embolism before stomata
444 completely close. Such a strategy is only likely to be viable in environments with less frequent or
445 intense drought. Taken together, these patterns suggest that drought adaptation in *T. triandra* relies
446 more on drought avoidance through conservative regulation of plant water status rather than
447 greater xylem embolism resistantance.

448 The positive correlation between temperature and P_{50} suggests increased embolism
449 resistance is adaptive in warmer climates, where high evaporative demand and increased
450 transpiration generate strongly negative xylem water potentials. This pattern of increasing embolism
451 resistance with increasing temperature has been documented in other herbaceous (Huang *et al.*,
452 2024) and woody species (Trueba *et al.*, 2017; Guan *et al.*, 2023), as well as in different provenances
453 of *Corymbia calophylla* (Blackman *et al.*, 2017). However, temperature-P_{50} relationships in woody
454 species vary considerably across studies, with some finding no relationship (Larter *et al.*, 2017; Li *et*
455 *al.*, 2018; López *et al.*, 2021; Peters *et al.*, 2021, p. 202) or even negative correlations on a global
456 scale (Nardini & Luglio, 2014). This variation may partly reflect confounding effects of temperature
457 and precipitation in many studies, making it difficult to isolate the independent effects of each
458 climate variable. In our study, low collinearity between these factors allowed us to separate their
459 independent effects. Additionally, variation in temperature-P_{50} relationships may reflect the
460 different selective pressures operating at temperature extremes: while high embolism resistance
461 protects against water stress-induced cavitation in hot environments, it may also provide protection
462 against freeze-thaw induced embolism in very cold environments (Davis *et al.*, 1999; Pittermann &
463 Sperry, 2006; Hartill *et al.*, 2023). Since the *T. triandra* populations in our study originated from
464 regions that rarely see severe freezing events during the growing season, the observed increase in
465 embolism resistance with increasing temperature likely reflects adaptations to hydraulic stress due
466 to high VPD in warm climates rather than to freeze-thaw embolism tolerance in cooler climates.

Additionally, perennial grasses may senesce frost-damaged leaves and resprout from basal meristems once temperatures are more suitable, weakening selection pressure for freeze-thaw embolism resistance.

Consistent with our second hypothesis, plants from warm sites exhibited higher hydraulic conductance, aligning with previous findings in woody angiosperms (Nardini & Luglio, 2014; Larter *et al.*, 2017; Peters *et al.*, 2021). Plants growing in hot, high-VPD environments may require greater hydraulic capacity to match elevated evaporative demand without incurring excessively negative leaf water potentials (Brodribb & Jordan, 2008; Osborne & Sack, 2012; Scoffoni *et al.*, 2016). Beyond maintaining plant water balance, higher K_{leaf} also facilitates greater leaf transpirational cooling in hot environments (Blonder *et al.*, 2023). Notably, plants from warm sites exhibited both high embolism resistance and high K_{leaf}, suggesting that hydraulic safety and efficiency is co-optimized in these environments rather than traded off. *T. triandra* plants from drier climates also exhibited higher K_{leaf} than those from wetter climates. While this pattern contrasts with a large meta-analysis involving 130 woody species (Nardini & Luglio, 2014) it aligns with findings in closely related *Caragana* species (Yao *et al.*, 2021) and reflects the complex, scale-dependent nature of hydraulic trait relationships. Within-genus variation in hydraulic conductivity-precipitation relationships has been documented in *Quercus* (Guan *et al.*, 2023) and importantly, stem and leaf hydraulic conductivity can show opposing trends with precipitation (López *et al.*, 2016, 2021). Our findings, which were at the leaf-level, are consistent with other studies showing declining K_{leaf} with increasing precipitation (López *et al.*, 2016, 2021; Yao *et al.*, 2021) and may represent an adaptive strategy that allows plants to maximise water uptake after sporadic rainfall events.

Anatomical traits showed limited relationships with climate. We found no relationship between xylem anatomical traits and precipitation, however we found that plant from warmer site had larger minor vein vessels, suggesting that temperature may exert greater selective pressure than precipitation on these traits across *T. triandra* populations. These patterns accord with our second hypothesis and align with observations in woody species where site precipitation had little effect on vein diameter but temperature showed a positive relationship with vessel diameter (Morris *et al.*, 2018; Olson *et al.*, 2018). Our third hypothesis that vessel diameter increases with temperature was partially supported, with plants from hotter environments only exhibiting significantly larger vessels in minor veins. Notably, K_{leaf} showed no significant relationship with major or minor vessel diameter and was *negatively* correlated with minor vein density —opposite to typical predictions linking higher vein density with greater conductance (Bayramzadeh et al., 2011; Fontes et al., 2022; Zhang et al., 2024). These patterns suggest that K_{leaf} in *T. triandra* is primarily determined by outside-xylem

conductance (K_{ox}), , which includes pathways through the vascular parenchyma, bundle sheath, and mesophyll tissues (Scoffoni *et al.*, 2017, 2023) rather than xylem vessel anatomy.

Photosynthetic capacity (A_{max}) showed no significant relationship with climate-of-origin however, g_{smax} was significantly lower in plants from hotter and drier environments. Intrinsically lower rates of stomatal conductance under hot and dry environments may be an adaptation to mitigate water loss from high VPD and low water availability respectively.

Hydraulic Trait Coordination and Implications for Drought Adaptation

We did not observe a negative correlation between P_{50} and K_{leaf} across populations (Fig. 5A); in fact plants from warm sites exhibited both high embolism resistance and high K_{leaf}. While this pattern is in contrast to the proposed safety-efficiency trade-off, which posits that higher hydraulic efficiency comes at the cost of reduced xylem safety (Hacke *et al.*, 2006; Gleason *et al.*, 2016), our results align with emerging evidence that the trade-off may be tissue-specific. Previous research has shown that the safety vs efficiency tradeoff is primarily present at the stem level but not at leaf level in closely related *Euphorbiaceae* species (Chen *et al.*, 2009) and across populations of *Atriplex Canescens* (Hao *et al.*, 2013). In stems, trade-offs between hydraulic efficiency and embolism resistance arise from xylem anatomical constraints, where vessel diameter and pit membrane properties create inherent conflicts between conductivity and embolism resistance (Wheeler et al., 2005; Sperry et al., 2006; Pittermann, 2010; Gleason et al., 2016; Pfautsch et al., 2016). In leaves however, Scoffoni & Sack, (2017) demonstrated that outside-xylem pathways (K_{ox}) contribute substantially to hydraulic resistance and determine leaf hydraulic decline during drought. Importantly, reductions in K_{ox} are generally recoverable once drought is alleviated (Scoffoni et al., 2014; Zhang et al., 2016), while xylem embolism is not (Skelton *et al.*, 2017; Johnson *et al.*, 2018). Hence, loss of K_{ox} may protect xylem from reaching the critically low water potentials that cause embolism and act as a protective mechanism (Scoffoni & Sack, 2017; Trifiló et al., 2016), potentially decoupling leaf hydraulic safety and efficiency. This protective function has been observed in previous studies that have shown that significant loss of K_{leaf} occurs well before the onset of xylem embolism (Corso *et al.*, 2020; Yao *et al.*, 2021) including in *T. triandra* specifically (Jacob *et al.*, 2022).

No significant relationship was observed between xylem embolism (P_{50}) and stomatal closure (g_{s90}), which contrasts with observations that stomatal regulation under drought is caused by embolism-induced reductions in K_{leaf} (Salleo *et al.*, 2000, p. 200; Nardini & Salleo, 2000; Nardini *et*

532 *al.*, 2001, p. 200; Lo Gullo *et al.*, 2003; Brodribb & Holbrook, 2003; Tombesi *et al.*, 2014; Savi *et al.*,
533 2016; Bartlett *et al.*, 2016; Torres-Ruiz *et al.*, 2019) but is more consistent with recent findings on
534 herbaceous species which observed no coordination between xylem embolism and stomatal closure
535 (Corso *et al.*, 2020; Jacob *et al.*, 2022). By contrast, Ψ_{TLP} was strongly coordinated with g_{s90},
536 reinforcing turgor loss as a key driver of stomatal closure (Salleo *et al.*, 2000; Bartlett *et al.*, 2012,
537 2014). We observed a positive relationship between Ψ_{TLP} and g_{smax},as plants that have lower g_{smax}
538 lose turgor at less negative water potential. While this relationship is in contrast to the findings of
539 Henry *et al.* (2019) on 15 tree and shrub species, it is similar to the trend observed by Li *et al.* (2018)
540 in 12 Australian tree species. Our results suggest that *T. triandra* plants adapted to dry environments
541 use a combination of low stomatal conductance and early loss of turgor to survive drought.

542 We found no evidence for coordination between leaf hydraulic conductance and leaf gas
543 exchange traits; in fact, we found a strong negative relationship between K_{leaf}, and g_{smax} and K_{leaf} and
544 A_{max}. These findings were unexpected given the tight coordination between hydraulic traits and gas
545 exchange reported in the literature (Franks, 2006; Brodribb & Holbrook, 2006; Brodribb *et al.*, 2007;
546 Mitchell *et al.*, 2014; Ocheltree *et al.*, 2016; Xiong *et al.*, 2018). However, decoupling between K_{leaf}
547 and leaf gas exchange has been reported in a number of recent studies on C_4 grasses (Ocheltree *et*
548 *al.*, 2016; Zhou *et al.*, 2020; Pathare *et al.*, 2020; Baird *et al.*, 2025). In the warm and arid
549 environments where C4 plants dominate selection for high WUEi via lower stomatal conductance
550 (Zhou et al., 2021) is likely advantageous. This decoupling of hydraulic traits and gas exchange may
551 also reflect the capacity of perennial grasses to transport more water than required to sustain
552 maximal assimilation rates (Holloway-Phillips & Brodribb, 2011; Baird *et al.*, 2025). Unlike C3 species,
553 C_4 grasses do not require high K_{leaf} to sustain photosynthetic rates, as their carbon-concentrating
554 mechanism allows high photosynthesis despite lower g_s and higher operating Ψ_{leaf} (Taylor *et al.*,
555 2011; Zhou *et al.*, 2020; Baird *et al.*, 2025). Additionally, Bucci et al. (2019) found that the
556 relationship between K_{leaf} and assimilation varied depending on the time of day, suggesting that the
557 K_{leaf}-leaf gas exchange relationship may be more context-dependent than previously thought.

558 Vessel wall thickness was not correlated with P_{50}, which contrasts with embolism resistance
559 mechanisms described in another grass species *Dactylis glomerata* (Volaire et al., 2018). Surprisingly,
560 plants with larger vessels exhibited greater embolism resistance, suggesting that mechanisms
561 unrelated to vessel wall dimensions drive embolism resistance in *T. triandra*. Previous research has
562 suggested that embolism resistance in angiosperms is primarily driven by pit level traits, including
563 intervessel pit membrane thickness, pit diameter and the number of inter-vessel pits per vessel
564 (Jansen *et al.*, 2009; Li *et al.*, 2016; Kaack *et al.*, 2019; Thonglim *et al.*, 2021). These pit traits are
565 often assumed to constrain vessel diameter due to the commonly observed trade-off between

566 hydraulic safety and efficiency, with narrower vessels typically associated with greater embolism
567 resistance. However, the positive relationship between vessel diameter and embolism resistance
568 observed in this study suggests that pit-level traits conferring safety (e.g. thicker or less porous pit
569 membranes) may, in this case, co-occur with wider vessels. This suggests that vessel size–safety
570 trade-offs may be relaxed or absent within *T. triandra*, highlighting the potential for adaptation to
571 enable both high efficiency and high safety in xylem function in populations from warmer climates.
572 The lack of clear relationship between vessel diameter and K_{leaf} and the striking positive relationship
573 between vessel size and P_{50} also echoes recent work highlighting the significant influence of outside
574 xylem factors on leaf hydraulic function (Scoffoni *et al.*, 2017, 2023).

575

576 ***Conclusion***

577 Our study into the hydraulic strategies of the widespread perennial grass, *T. triandra*, highlights the
578 complex interplay between hydraulic traits, stomatal regulation, and xylem anatomy in shaping
579 climate adaptation. Rather than having evolved high embolism resistance, we found that *T. triandra*
580 populations from drier climates employ a conservative water-use strategy —lower stomatal
581 conductance, earlier stomatal closure and turgor loss (less negative g_{s90} and Ψ_{TLP} respectively) and
582 larger stomatal safety margins — potentially limiting strongly negative leaf water potentials and
583 reducing embolism risk during dry conditions. By contrast, plants from warmer climates exhibited a
584 combination of high hydraulic conductance and high embolism resistance, enabling rapid water
585 transport to match evaporative demand and sustain transpirational cooling, while reducing the risk
586 of hydraulic failure. Our results reveal substantial within-species variation in hydraulic traits and
587 provide a more nuanced understanding of the mechanisms enabling success in hot and dry
588 environments; these contrasting strategies may help inform climate models aimed at predicting
589 plant responses to intensifying drought and warming, particularly in grassland ecosystems.

590

591 **Acknowledgements**

592 We thank Dr Alan Humphries from the Australian Pastures Genebank for advice on germinating *T.*
593 *triandra* and for providing seed sources that helped make this project possible. VKJ, IJW, CJB, EF, ACL
594 TB and ES acknowledge support from the Australian Research Council (CE200100015).

595

596 **Competing interests**

No competing interests are declared.

Author contributions

VJ and IJW led project design, experimental work and manuscript preparation, with strong support from CJB and BC. ACL, TB and ES assisted with data collection. All authors discussed results, contributed ideas and text to multiple versions of the manuscript, and approved the final version.

Figures and Tables

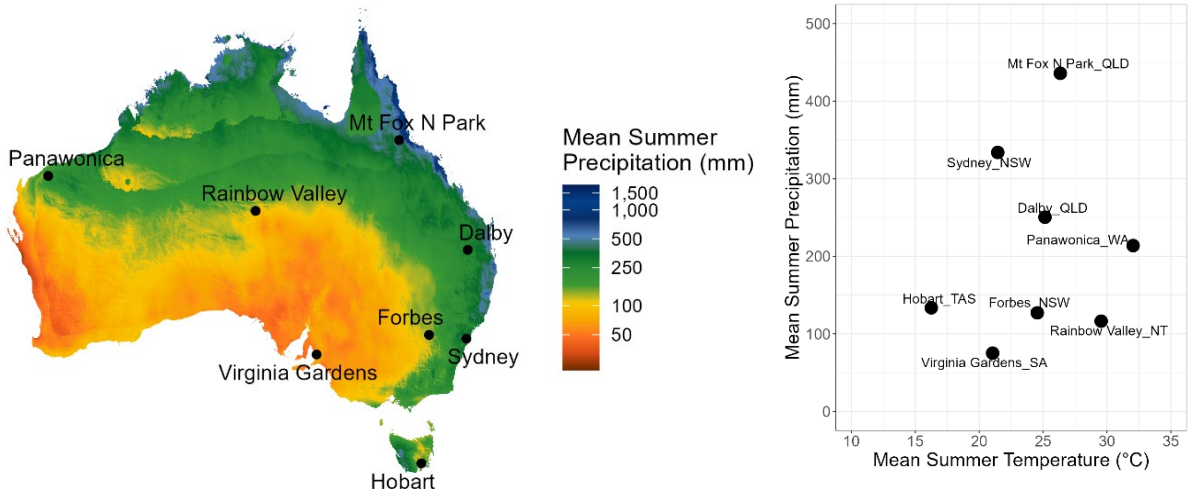

(A) (B)

FIGURE 1. Climate-of-origin of populations used in this study. (A) Mean summer precipitation; mm) across Australia; populations represented by black dots (•). (B) Scatter plot illustrating the two key climatic predictors, with Summer temperature (°C) on the x-axis and mean summer precipitation on the y-axis.

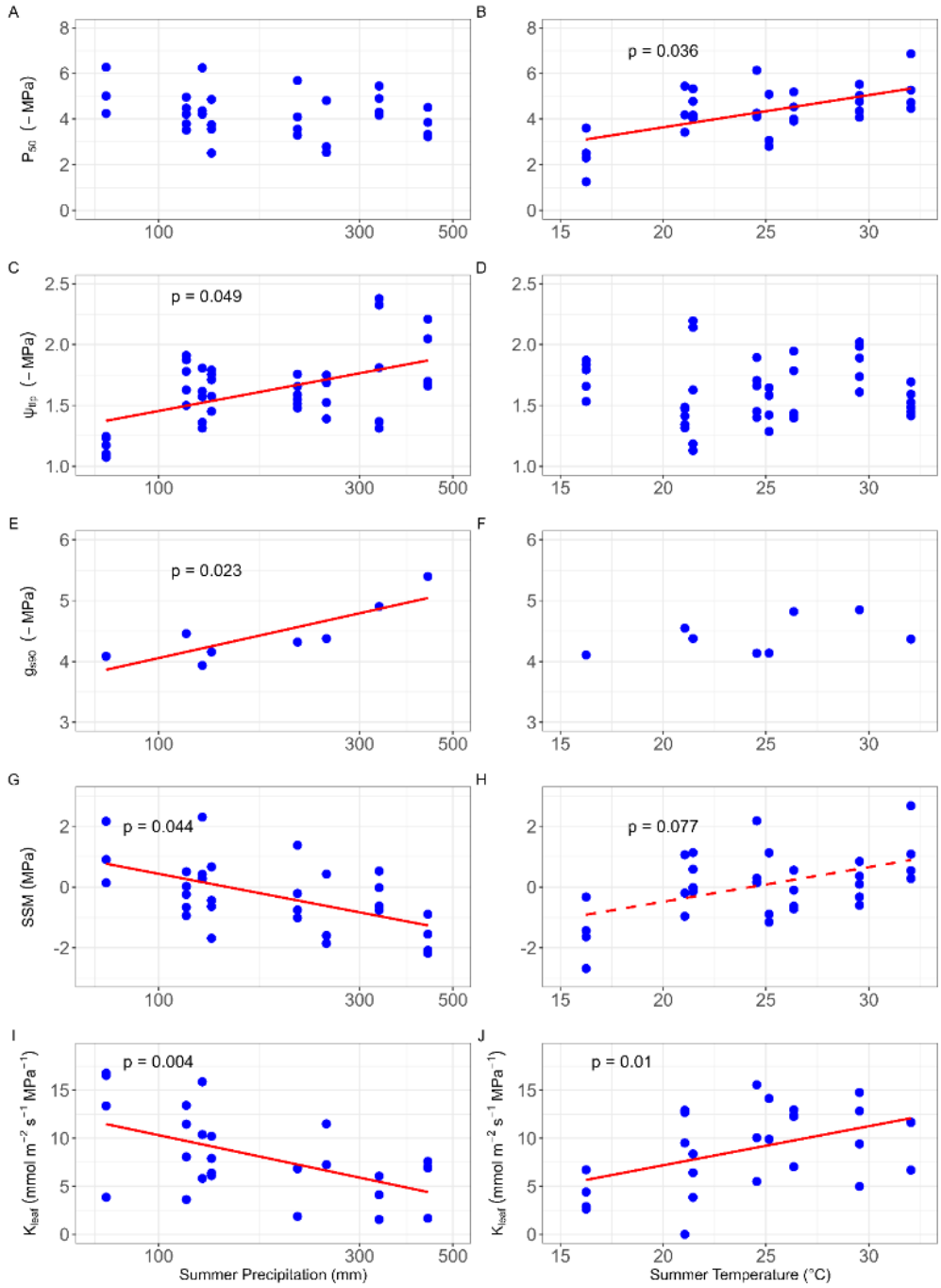

Figure 2. Partial residual plots showing the independent relationships between climate-of-origin and hydraulic traits across populations of *T. triandra*. Relationships between mean summer precipitation (A, C, E, G, I) and mean summer temperature (B, D, F, H, J) with (A, B) water potential at 50% xylem embolism (P_{50}), (C, D) water potential at leaf turgor loss (Ψ_{TLP}), (E, F) water potential at 90% stomatal closure (g_{s90}), (G, H) stomatal safety margin (SSM, Δ g_{s90} & P_{50}), and (I, J) leaf hydraulic conductance (K_{leaf}). Fitted lines are derived from linear mixed-effects models using mean data from individual plants, with population as a random effect. Partial residuals were obtained from a corresponding multiple regression model, without the random effect, to visualize the independent effects of each climate variable. Solid red lines indicate significant linear regression fits ($p < 0.05$), while dashed red lines denote marginally significant relationships ($p < 0.1$). Mean summer precipitation was log-transformed to standardize coefficients and back-transformed for visualization.

610

611

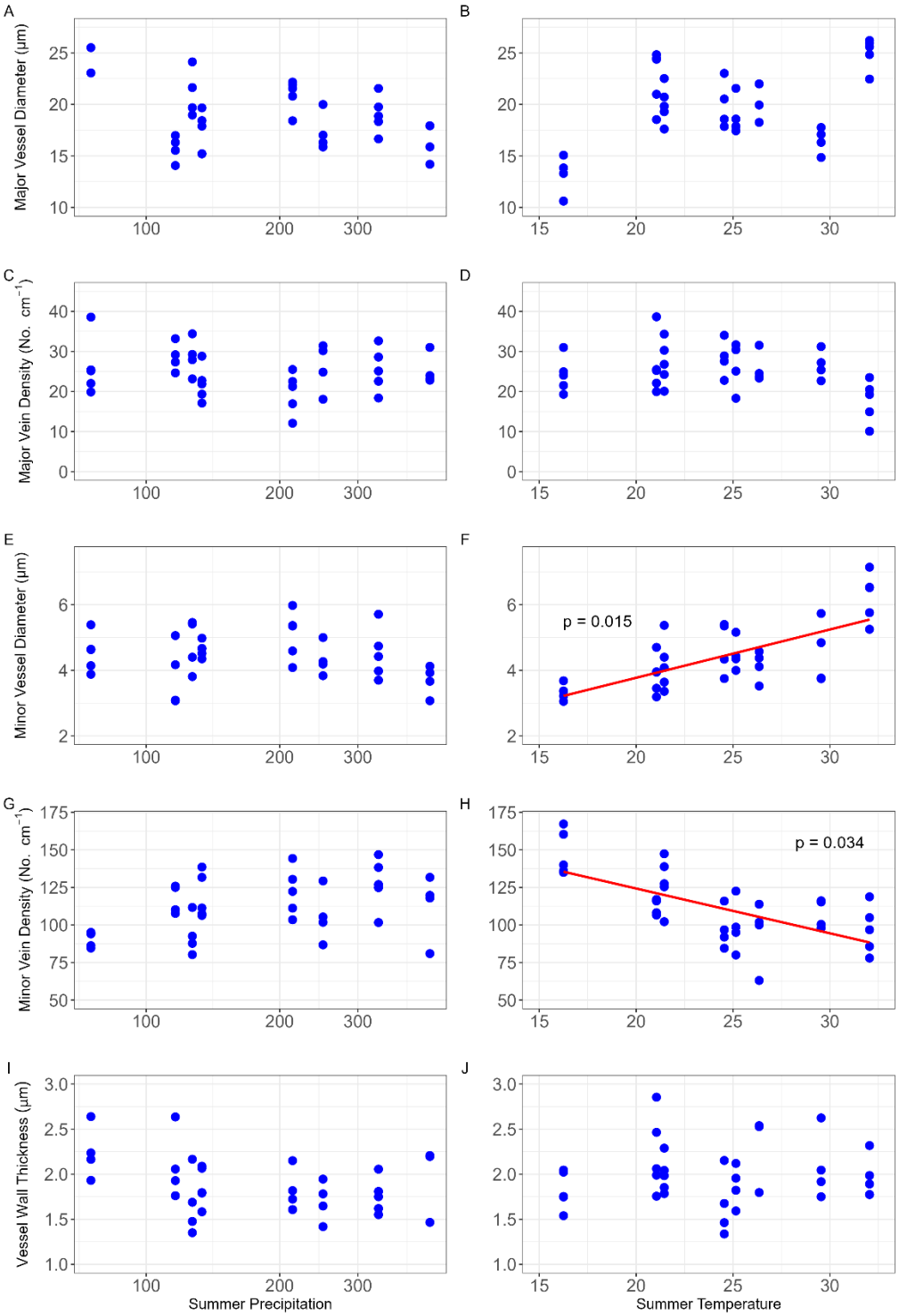

Figure 3: Partial residual plots showing the independent relationships between climate-of-origin and xylem anatomical traits across populations of *T. triandra*. Relationships between mean summer precipitation (A, C, E, G) and mean summer temperature (B, D, F, H) with (A, B) major vessel diameter, (C, Dmajor vein density, (E, F) minor vessel diameter and (G, H) minor vein density. Fitted lines are derived from linear mixed-effects models using mean data from individual plants, with population as a random effect. Partial residuals were obtained from a corresponding multiple regression model, without the random effect, to visualize the independent effects of each climate variable. Solid red lines indicate significant linear regression fits ($p < 0.05$). Mean

summer precipitation was log-transformed to standardize coefficients and back-transformed for visualization.

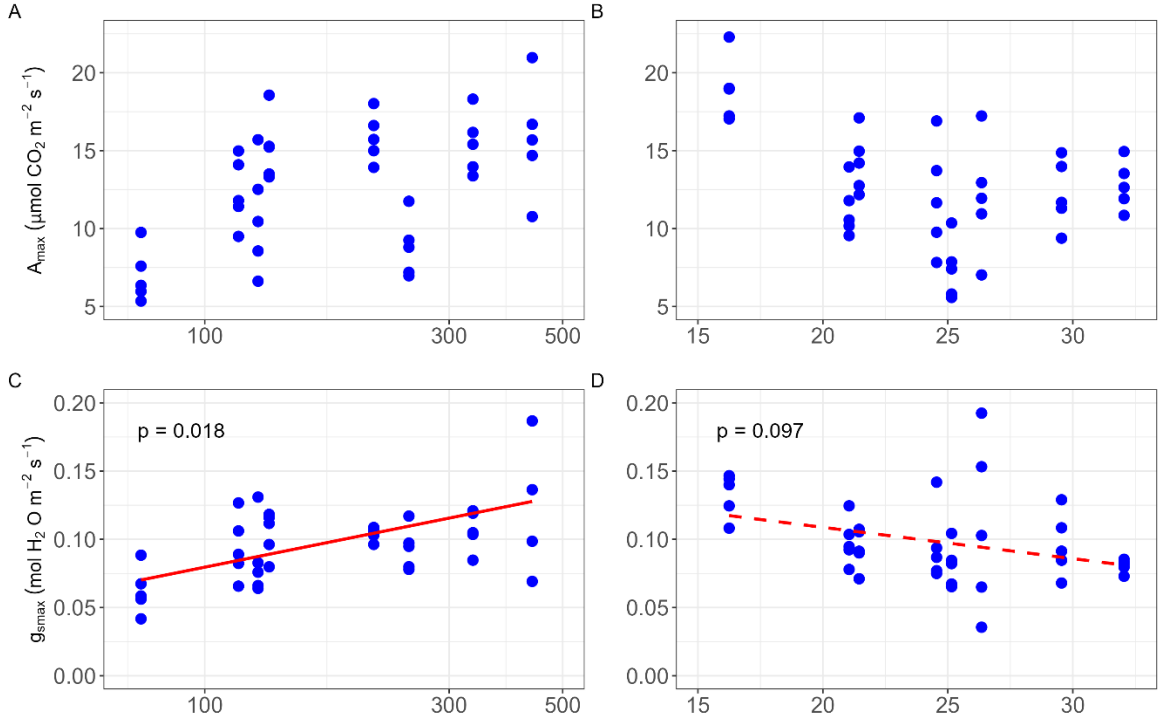

Figure 4. Partial residual plots showing the independent relationships between climate-of-origin and leaf gas exchange traits across populations of *T. triandra*. Relationships between mean summer precipitation (A, C) and mean summer temperature (B, D) with (A, B) maximum rates of light saturated photosynthesis (A_{max}), (C, D) and maximum rates of stomatal conductance (g_{smax}). Fitted lines are derived from linear mixed-effects models using mean data from individual plants, with population as a random effect. Partial residuals were obtained from a corresponding multiple regression model, without the random effect, to visualize the independent effects of each climate variable. Solid red lines indicate significant linear regression fits ($p < 0.05$), while dashed red lines denote marginally significant relationships ($p < 0.1$). Mean summer precipitation was log-transformed to standardize coefficients and back-transformed for visualization.

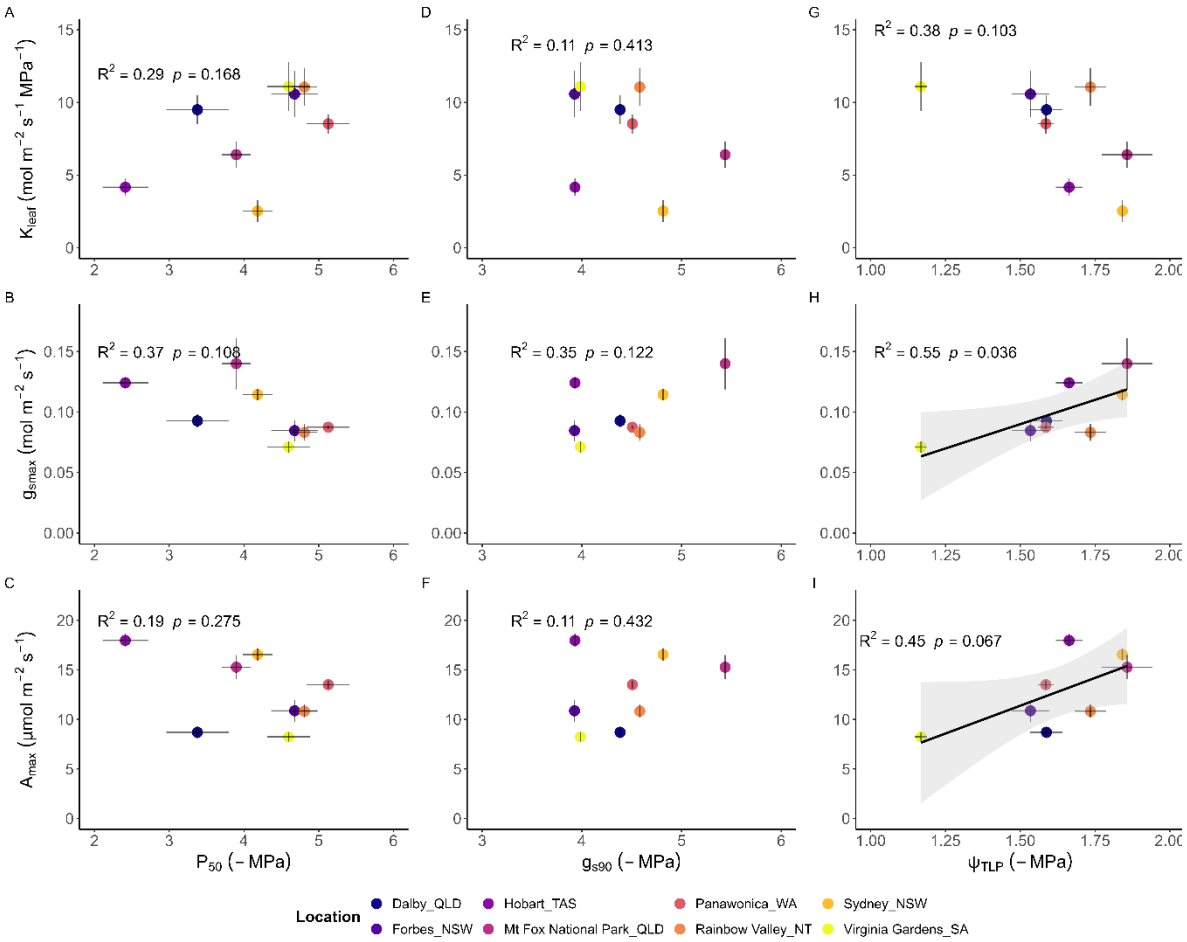

Figure 5: Linear regressions examining relationships between *safety* and *efficiency* traits across populations of *T. triandra*. Correlation between xylem embolism resistance (P_{50}) and (A) hydraulic conductivity (K_{leaf}), (B) maximum stomatal conductance (g_{smax}) and (C) maximum photosynthetic rate (A_{max}). Relationships between xylem water potential at 90% stomatal closure (g_{s90}) and (D) K_{leaf}, (E) g_{smax} and (F) A_{max}. Relationship between leaf water potential at turgor loss (Ψ_{TLP}) and (G) K_{leaf}, (H) g_{smax} and (I) A_{max} . Solid lines and shaded 95% confidence bands are displayed only for statistically significant relationships ($P < 0.1$). Adjusted R^2 values and P-values (derived from Pearson correlations, equivalent to simple OLS tests) are likewise displayed only when $p < 0.1$. Error bars denote ± standard error of the mean; colours denote different populations.

626

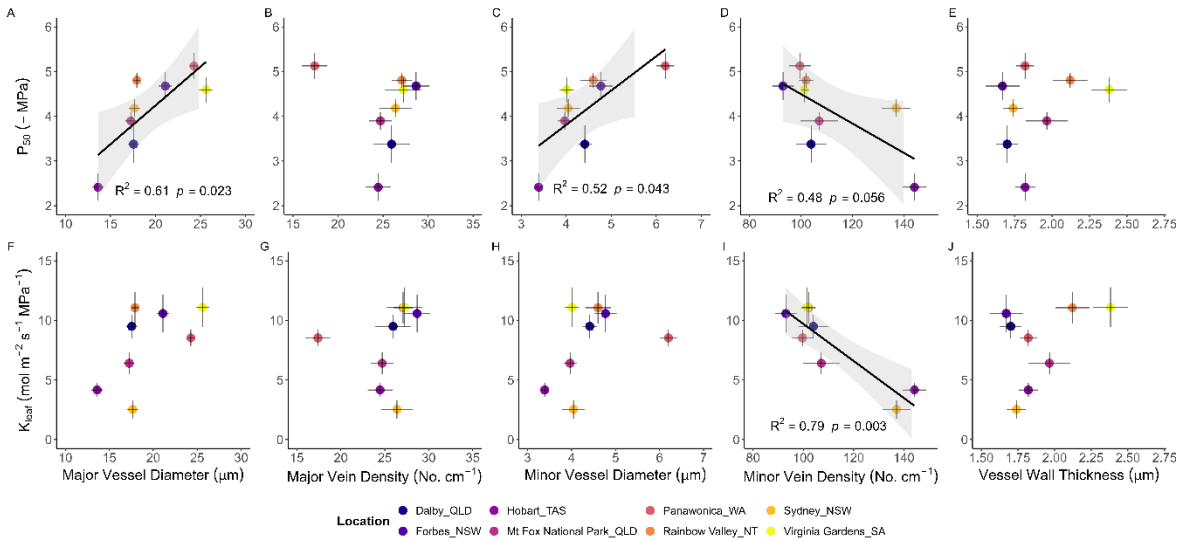

Figure 6: Linear regressions examining relationships between hydraulic traits and xylem anatomy across populations of *T. triandra*. (A–E) Correlations between xylem embolism resistance (P_{50}), (F–J) leaf hydraulic conductance (K_{leaf}) and major vessel diameter(A, F), major vessel density, (B, G) minor vessel diameter (C, H), minor vein density (D, I), and major vessel wall thickness (E, J). Solid lines and shaded 95% confidence bands are displayed only for statistically significant relationships ($P < 0.1$). Adjusted R^2 values and P-values (derived from Pearson correlations, equivalent to simple OLS tests) are likewise displayed only when $p < 0.1$. Error bars denote ± standard error of the mean; colours denote different populations.

627

628

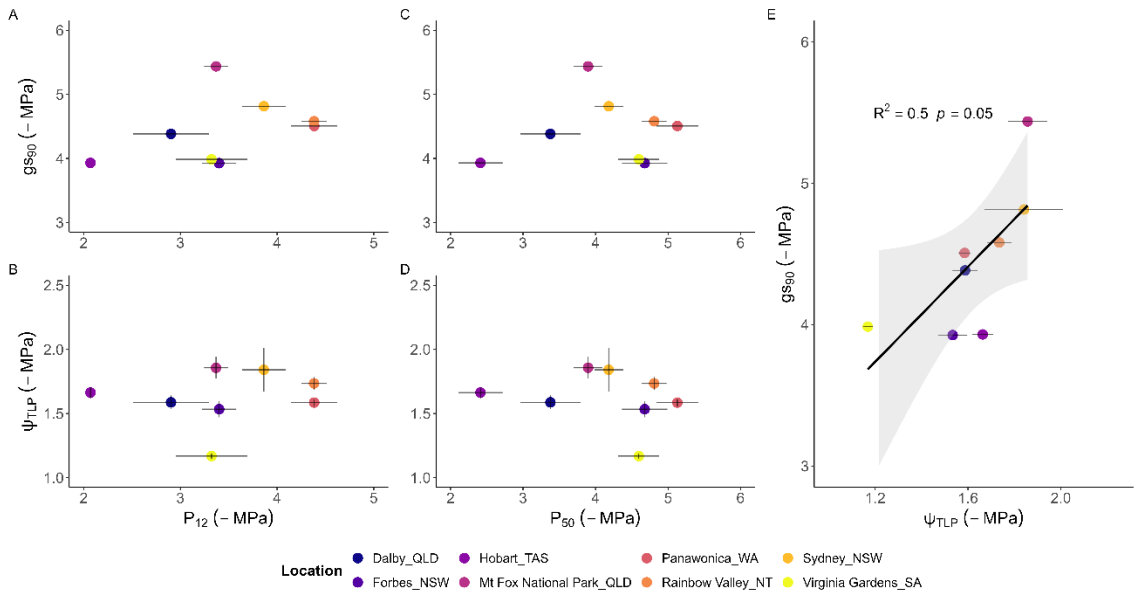

Figure 7. Linear regressions examining relationships between hydraulic vulnerability and water potential at turgor loss and stomatal closure across *T. triandra* populations. Correlations between water potential at 12% xylem embolism (P_{12}) and (A) water potential at 90% stomatal closure (g_{s90}) and (B) leaf water potential at turgor loss (Ψ_{TLP}). Correlations between water potential at 50% xylem embolism (P_{50}) and (C) g_{s90} and (D) Ψ_{TLP}. Correlation between Ψ_{TLP} and (E) g_{s90} . Solid lines and shaded 95% confidence bands are displayed only for statistically significant relationships (P <

0.1). Adjusted R^2 values and P-values (derived from Pearson correlations, equivalent to simple OLS tests) are likewise displayed only when $p < 0.1$. Error bars denote ± standard error of the mean; colours denote different populations.

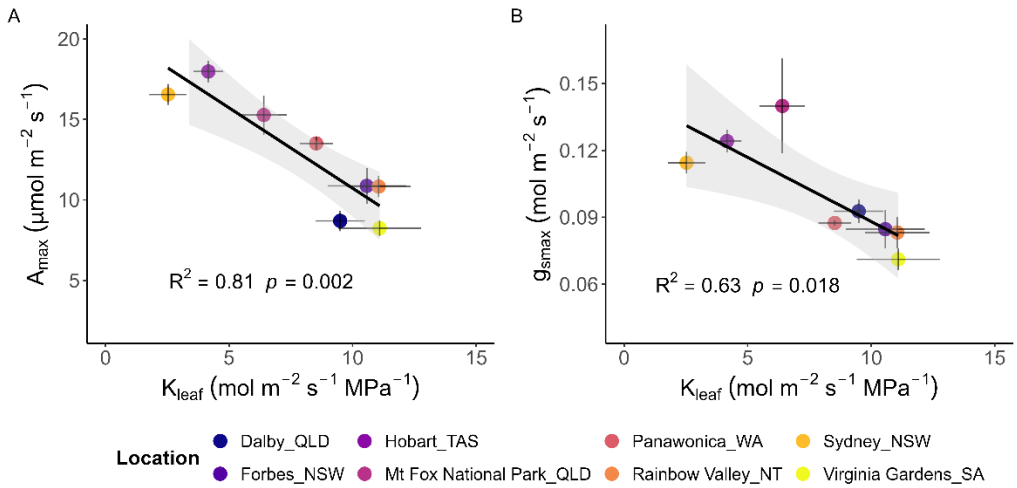

Figure 8: Linear regressions examining the relationships between leaf hydraulic conductance and leaf gas exchange across populations of *T. triandra*. Correlations between leaf hydraulic conductance (K_{leaf}) and (A) maximum photosynthetic rate (A_{max}) and (B) maximum stomatal conductance (g_{smax}). Solid lines and shaded 95% confidence bands are displayed only for statistically significant relationships ($P < 0.1$). Adjusted R^2 values and P-values (derived from Pearson correlations, equivalent to simple OLS tests) are likewise displayed only when $p < 0.1$. Error bars denote ± standard error of the mean; colours denote different populations.

REFERENCES

Arthan W, Morales-Fierro V, Vorontsova MS, Kellogg EA, Mitchley J, Lehmann CER. **2022**. *Heteropogon - Themeda* grasses evolve to occupy either tropical grassland or wetland biomes. *Journal of Systematics and Evolution* **60**: 653–674.

Baird AS, Taylor SH, Pasquet-Kok J, Vuong C, Zhang Y, Watcharamongkol T, Cochard H, Scoffoni C, Edwards EJ, Osborne CP, *et al.* 2025. Resolving the contrasting leaf hydraulic adaptation of C_3 and C_4 grasses. *New Phytologist* **245**: 1924–1939.

Balachowski JA, Bristiel PM, Volaire FA. **2016**. Summer dormancy, drought survival and functional resource acquisition strategies in California perennial grasses. *Annals of Botany* **118**: 357–368.

Bartlett MK, Klein T, Jansen S, Choat B, Sack L. **2016**. The correlations and sequence of plant stomatal, hydraulic, and wilting responses to drought. *Proceedings of the National Academy of Sciences* **113**: 13098–13103.

Bartlett MK, Scoffoni C, Ardy R, Zhang Y, Sun S, Cao K, Sack L. **2012**. Rapid determination of comparative drought tolerance traits: using an osmometer to predict turgor loss point. *Methods in Ecology and Evolution* **3**: 880–888.

Bartlett MK, Zhang Y, Kreidler N, Sun S, Ardy R, Cao K, Sack L. **2014**. Global analysis of plasticity in turgor loss point, a key drought tolerance trait (J Gurevitch, Ed.). *Ecology Letters* **17**: 1580–1590.

Bayramzadeh V, Attarod P, Ahmadi MT, Rezaee Amruabadi SH, Kubo T. **2011**. Does the climate of the origin control anatomical characteristics of the vessel elements as well as different foliar traits in Fagus crenata? *Journal of Forest Science* **57**: 377–383.

Bjorkman AD, Myers-Smith IH, Elmendorf SC, Normand S, Rüger N, Beck PSA, Blach-Overgaard A, Blok D, Cornelissen JHC, Forbes BC, *et al.* 2018. Plant functional trait change across a warming tundra biome. *Nature* **562**: 57–62.

Blackman CJ. **2018**. Leaf turgor loss as a predictor of plant drought response strategies. *Tree Physiology* **38**: 655–657.

Blackman CJ, Aspinwall MJ, Tissue DT, Rymer PD. **2017**. Genetic adaptation and phenotypic plasticity contribute to greater leaf hydraulic tolerance in response to drought in warmer climates. *Tree Physiology* **37**: 583–592.

Blackman CJ, Gleason SM, Chang Y, Cook AM, Laws C, Westoby M. **2014**. Leaf hydraulic vulnerability to drought is linked to site water availability across a broad range of species and climates. *Annals of Botany* **114**: 435–440.

Blonder BW, Aparecido LMT, Hultine KR, Lombardozzi D, Michaletz ST, Posch BC, Slot M, Winter K. **2023**. Plant water use theory should incorporate hypotheses about extreme environments, population ecology, and community ecology. *New Phytologist* **238**: 2271–2283.

Bourne AE, Creek D, Peters JMR, Ellsworth DS, Choat B. **2017**. Species climate range influences hydraulic and stomatal traits in Eucalyptus species. *Annals of Botany* **120**: 123–133.

Brodribb TJ, Feild TS, Jordan GJ. **2007**. Leaf Maximum Photosynthetic Rate and Venation Are Linked by Hydraulics. *Plant Physiology* **144**: 1890–1898.

Brodribb TJ, Holbrook NM. **2003**. Stomatal Closure during Leaf Dehydration, Correlation with Other Leaf Physiological Traits. *Plant Physiology* **132**: 2166–2173.

Brodribb TJ, Holbrook NM. **2006**. Declining hydraulic efficiency as transpiring leaves desiccate: two types of response*. *Plant, Cell & Environment* **29**: 2205–2215.

Brodribb TJ, Jordan GJ. **2008**. Internal coordination between hydraulics and stomatal control in leaves. *Plant, Cell & Environment* **31**: 1557–1564.

Brodribb TJ, Skelton RP, McAdam SAM, Bienaimé D, Lucani CJ, Marmottant P. **2016**. Visual quantification of embolism reveals leaf vulnerability to hydraulic failure. *New Phytologist* **209**: 1403–1409.

Chen J-W, Zhang Q, Li X-S, Cao K-F. **2009**. Independence of stem and leaf hydraulic traits in six Euphorbiaceae tree species with contrasting leaf phenology. *Planta* **230**: 459–468.

Chen Z, Zhu S, Zhang Y, Luan J, Li S, Sun P, Wan X, Liu S. **2020**. Tradeoff between storage capacity and embolism resistance in the xylem of temperate broadleaf tree species. *Tree Physiology* **40**: 1029–1042.

Choat B, Brodribb TJ, Brodersen CR, Duursma RA, López R, Medlyn BE. **2018**. Triggers of tree mortality under drought. *Nature* **558**: 531–539.

Choat B, Cobb AR, Jansen S. **2008**. Structure and function of bordered pits: new discoveries and impacts on whole-plant hydraulic function. *New Phytologist* **177**: 608–626.

Choat B, Jansen S, Brodribb TJ, Cochard H, Delzon S, Bhaskar R, Bucci SJ, Feild TS, Gleason SM, Hacke UG, *et al.* 2012. Global convergence in the vulnerability of forests to drought. *Nature* **491**: 752–755.

Churchill AC, Zhang H, Fuller KJ, Amiji B, Anderson IC, Barton CVM, Carrillo Y, Catunda KLM, Chandregowda MH, Igwenagu C, *et al.* 2022. Pastures and Climate Extremes: Impacts of Cool Season Warming and Drought on the Productivity of Key Pasture Species in a Field Experiment. *Frontiers in Plant Science* **13**: 836968.

Corso D, Delzon S, Lamarque LJ, Cochard H, Torres-Ruiz JM, King A, Brodribb T. **2020**. Neither xylem collapse, cavitation, or changing leaf conductance drive stomatal closure in wheat. *Plant, Cell & Environment* **43**: 854–865.

Craine JM, Ocheltree TW, Nippert JB, Towne EG, Skibbe AM, Kembel SW, Fargione JE. **2013**. Global diversity of drought tolerance and grassland climate-change resilience. *Nature Climate Change* **3**: 63–67.

Davis SD, Sperry JS, Hacke UG. **1999**. The relationship between xylem conduit diameter and cavitation caused by freezing. *American Journal of Botany* **86**: 1367–1372.

Dunning LT, Liabot A-L, Olofsson JK, Smith EK, Vorontsova MS, Besnard G, Simpson KJ, Lundgren MR, Addicott E, Gallagher RV, *et al.* 2017. The recent and rapid spread of *Themeda triandra*. *Botany Letters* **164**: 327–337.

Fontes CG, Pinto-Ledezma J, Jacobsen AL, Pratt RB, Cavender-Bares J. **2022**. Adaptive variation among oaks in wood anatomical properties is shaped by climate of origin and shows limited plasticity across environments. *Functional Ecology* **36**: 326–340.

Franks PJ. **2006**. Higher rates of leaf gas exchange are associated with higher leaf hydrodynamic pressure gradients. *Plant, Cell & Environment* **29**: 584–592.

Gleason SM, Westoby M, Jansen S, Choat B, Hacke UG, Pratt RB, Bhaskar R, Brodribb TJ, Bucci SJ, Cao K-F, *et al.* 2016. Weak tradeoff between xylem safety and xylem-specific hydraulic efficiency across the world's woody plant species. *New Phytologist* **209**: 123–136.

Griffin-Nolan RJ, Bushey JA, Carroll CJW, Challis A, Chieppa J, Garbowski M, Hoffman AM, Post AK, Slette IJ, Spitzer D, *et al.* 2018. Trait selection and community weighting are key to understanding ecosystem responses to changing precipitation regimes (C Fox, Ed.). *Functional Ecology* **32**: 1746–1756.

Griffin-Nolan RJ, Sandel B. **2023**. Global intraspecific trait–climate relationships for grasses are linked to a species' typical form and function. *Ecography* **2023**: e06586.

Guan X, Wen Y, Zhang Y, Chen Z, Cao K-F. **2023**. Stem hydraulic conductivity and embolism resistance of *Quercus* species are associated with their climatic niche (J Martinez-Vilalta, Ed.). *Tree Physiology* **43**: 234–247.

Hacke UG, Sperry JS, Pockman WT, Davis SD, McCulloh KA. **2001**. Trends in wood density and structure are linked to prevention of xylem implosion by negative pressure. *Oecologia* **126**: 457–461.

Hacke UG, Sperry JS, Wheeler JK, Castro L. **2006**. Scaling of angiosperm xylem structure with safety and efficiency. *Tree Physiology* **26**: 689–701.

Hao G-Y, Lucero ME, Sanderson SC, Zacharias EH, Holbrook NM. **2013**. Polyploidy enhances the occupation of heterogeneous environments through hydraulic related trade-offs in Atriplex canescens (Chenopodiaceae). *New Phytologist* **197**: 970–978.

Hartill GE, Blackman CJ, Halliwell B, Jones RC, Holland BR, Brodribb TJ. **2023**. Cold temperature and aridity shape the evolution of drought tolerance traits in Tasmanian species of Eucalyptus. *Tree Physiology* **43**: 1493–1500.

Hartmann H, Link RM, Schuldt B. **2021**. A whole-plant perspective of isohydry: stem-level support for leaf-level plant water regulation (S Sevanto, Ed.). *Tree Physiology* **41**: 901–905.

Henry C, John GP, Pan R, Bartlett MK, Fletcher LR, Scoffoni C, Sack L. **2019**. A stomatal safety-efficiency trade-off constrains responses to leaf dehydration. *Nature Communications* **10**: 3398.

Hochberg U, Rockwell FE, Holbrook NM, Cochard H. **2018**. Iso/Anisohydry: A Plant–Environment Interaction Rather Than a Simple Hydraulic Trait. *Trends in Plant Science* **23**: 112–120.

Holloway-Phillips M, Brodribb TJ. **2011**. Minimum hydraulic safety leads to maximum water-use efficiency in a forage grass. *Plant, Cell & Environment* **34**: 302–313.

Hoover DL, Knapp AK, Smith MD. **2014**. Resistance and resilience of a grassland ecosystem to climate extremes. *Ecology* **95**: 2646–2656.

Huang R, Di N, Xi B, Yang J, Duan J, Li X, Feng J, Choat B, Tissue D. **2024**. Herb hydraulics: Variation and correlation for traits governing drought tolerance and efficiency of water transport. *Science of The Total Environment* **907**: 168095.

Huxman TE, Winkler DE, Mooney KA. **2022**. A common garden super-experiment: An impossible dream to inspire possible synthesis. *Journal of Ecology* **110**: 997–1004.

Jacob V, Choat B, Churchill AC, Zhang H, Barton CVM, Krishnananthaselvan A, Post AK, Power SA, Medlyn BE, Tissue DT. **2022**. High safety margins to drought-induced hydraulic failure found in five pasture grasses. *Plant, Cell & Environment* **45**: 1631–1646.

Jankowski A, Wyka TP, Żytkowiak R, Danusevičius D, Oleksyn J. **2019**. Does climate-related in situ variability of Scots pine (Pinus sylvestris L.) needles have a genetic basis? Evidence from common garden experiments. *Tree Physiology* **39**: 573–589.

Jansen S, Choat B, Pletsers A. **2009**. Morphological variation of intervessel pit membranes and implications to xylem function in angiosperms. *American Journal of Botany* **96**: 409–419.

Johnson KM, Jordan GJ, Brodribb TJ. **2018**. Wheat leaves embolized by water stress do not recover function upon rewatering. *Plant Cell and Environment* **41**: 2704–2714.

Kaack L, Altaner CM, Carmesin C, Diaz A, Holler M, Kranz C, Neusser G, Odstrcil M, Jochen Schenk H, Schmidt V, *et al.* 2019. Function and three-dimensional structure of intervessel pit membranes in angiosperms: a review (LA Donaldson, Ed.). *IAWA Journal* **40**: 673–702.

Karger DN, Conrad O, Böhner J, Kawohl T, Kreft H, Soria-Auza RW, Zimmermann NE, Linder HP, Kessler M. **2017**. Climatologies at high resolution for the earth's land surface areas. *Scientific Data* **4**: 170122.

Keep T, Sampoux J, Barre P, Blanco-Pastor J, Dehmer KJ, Durand J, Hegarty M, Ledauphin T, Muylle H, Roldán-Ruiz I, *et al.* 2021. To grow or survive: Which are the strategies of a perennial grass to face severe seasonal stress? (K McCulloh, Ed.). *Functional Ecology* **35**: 1145–1158.

Klein T. **2014**. The variability of stomatal sensitivity to leaf water potential across tree species indicates a continuum between isohydric and anisohydric behaviours (S Niu, Ed.). *Functional Ecology* **28**: 1313–1320.

Lamy J-B, Delzon S, Bouche PS, Alia R, Vendramin GG, Cochard H, Plomion C. **2014**. Limited genetic variability and phenotypic plasticity detected for cavitation resistance in a Mediterranean pine. *New Phytologist* **201**: 874–886.

Larter M, Pfautsch S, Domec J, Trueba S, Nagalingum N, Delzon S. **2017**. Aridity drove the evolution of extreme embolism resistance and the radiation of conifer genus *Callitris*. *New Phytologist* **215**: 97–112.

Lens F, Gleason SM, Bortolami G, Brodersen C, Delzon S, Jansen S. **2022**. Functional xylem characteristics associated with drought-induced embolism in angiosperms. *New Phytologist* **236**: 2019–2036.

Lens F, Picon-Cochard C, Delmas CE, Signarbieux C, Buttler A, Cochard H, Jansen S, Chauvin T, Chacon Doria L, Del Arco M, *et al.* 2016. Herbaceous angiosperms are not more vulnerable to drought-induced embolism than angiosperm trees. *Plant Physiology*: pp.00829.2016.

Li X, Blackman CJ, Choat B, Duursma RA, Rymer PD, Medlyn BE, Tissue DT. **2018**. Tree hydraulic traits are coordinated and strongly linked to climate-of-origin across a rainfall gradient. *Plant, Cell & Environment* **41**: 646–660.

Li S, Lens F, Espino S, Karimi Z, Klepsch M, Schenk HJ, Schmitt M, Schuldt B, Jansen S. **2016**. INTERVESSEL PIT MEMBRANE THICKNESS AS A KEY DETERMINANT OF EMBOLISM RESISTANCE IN ANGIOSPERM XYLEM. *IAWA Journal* **37**: 152–171.

Lo Gullo MA, Nardini A, Trifilò P, Salleo S. **2003**. Changes in leaf hydraulics and stomatal conductance following drought stress and irrigation in Ceratonia siliqua (Carob tree). *Physiologia Plantarum* **117**: 186–194.

López R, Cano FJ, Choat B, Cochard H, Gil L. **2016**. Plasticity in Vulnerability to Cavitation of Pinus canariensis Occurs Only at the Driest End of an Aridity Gradient. *Frontiers in Plant Science* **7**.

López R, Cano FJ, Martin-StPaul NK, Cochard H, Choat B. **2021**. Coordination of stem and leaf traits define different strategies to regulate water loss and tolerance ranges to aridity. *New Phytologist* **230**: 497–509.

Madani N, Kimball JS, Ballantyne AP, Affleck DLR, Van Bodegom PM, Reich PB, Kattge J, Sala A, Nazeri M, Jones MO, *et al.* 2018. Future global productivity will be affected by plant trait response to climate. *Scientific Reports* **8**: 2870.

Maherali H, Pockman WT, Jackson RB. **2004**. ADAPTIVE VARIATION IN THE VULNERABILITY OF WOODY PLANTS TO XYLEM CAVITATION. *Ecology* **85**: 2184–2199.

Male D, Hunt J, Celestina C, Morgan J, Gupta D. **2022**. Themeda triandra as a perennial seed crop in south-eastern Australia: What are the agronomic possibilities and constraints, and future research needs? *Cogent Food & Agriculture*.

Maréchaux I, Bartlett MK, Sack L, Baraloto C, Engel J, Joetzjer E, Chave J. **2015**. Drought tolerance as predicted by leaf water potential at turgor loss point varies strongly across species within an Amazonian forest (K Kitajima, Ed.). *Functional Ecology* **29**: 1268–1277.

Markesteijn L, Poorter L, Paz H, Sack L, Bongers F. **2011**. Ecological differentiation in xylem cavitation resistance is associated with stem and leaf structural traits. *Plant, Cell & Environment* **34**: 137–148.

Martínez-Vilalta J, Cochard H, Mencuccini M, Sterck F, Herrero A, Korhonen JFJ, Llorens P, Nikinmaa E, Nolè A, Poyatos R, *et al.* 2009. Hydraulic adjustment of Scots pine across Europe. *New Phytologist* **184**: 353–364.

Martin-StPaul N, Delzon S, Cochard H. **2017**. Plant resistance to drought depends on timely stomatal closure. *Ecology Letters* **20**: 1437–1447.

McDowell N, Pockman WT, Allen CD, Breshears DD, Cobb N, Kolb T, Plaut J, Sperry J, West A, Williams DG, *et al.* 2008. Mechanisms of plant survival and mortality during drought: why do some plants survive while others succumb to drought? *New Phytologist* **178**: 719–739.

McSteen P, Kellogg EA. **2022**. Molecular, cellular, and developmental foundations of grass diversity. *Science*.

Mitchell PJ, O'Grady AP, Tissue DT, Worledge D, Pinkard EA. **2014**. Co-ordination of growth, gas exchange and hydraulics define the carbon safety margin in tree species with contrasting drought strategies. *Tree Physiology* **34**: 443–458.

Morris H, Gillingham MAF, Plavcová L, Gleason SM, Olson ME, Coomes DA, Fichtler E, Klepsch MM, Martínez-Cabrera HI, McGlinn DJ, *et al.* 2018. Vessel diameter is related to amount and spatial arrangement of axial parenchyma in woody angiosperms. *Plant, Cell & Environment* **41**: 245–260.

Nardini A, Luglio J. **2014**. Leaf hydraulic capacity and drought vulnerability: possible trade-offs and correlations with climate across three major biomes. *Functional Ecology* **28**: 810–818.

Nardini A, Salleo S. **2000**. Limitation of stomatal conductance by hydraulic traits: sensing or preventing xylem cavitation? *Trees* **15**: 14–24.

Nardini A, Tyree MT, Salleo S. **2001**. Xylem Cavitation in the Leaf of *Prunus laurocerasus* and Its Impact on Leaf Hydraulics. *Plant Physiology* **125**: 1700–1709.

Ocheltree TW, Nippert JB, Prasad PVV. **2016**. A safety vs efficiency trade-off identified in the hydraulic pathway of grass leaves is decoupled from photosynthesis, stomatal conductance and precipitation. *New Phytologist* **210**: 97–107.

Olson ME, Soriano D, Rosell JA, Anfodillo T, Donoghue MJ, Edwards EJ, León-Gómez C, Dawson T, Camarero Martínez JJ, Castorena M, *et al.* 2018. Plant height and hydraulic vulnerability to drought and cold. *Proceedings of the National Academy of Sciences* **115**: 7551–7556.

Osborne CP, Sack L. **2012**. Evolution of C4 plants: a new hypothesis for an interaction of CO2 and water relations mediated by plant hydraulics. *Philosophical Transactions of the Royal Society B: Biological Sciences* **367**: 583–600.

Pathare VS, Sonawane BV, Koteyeva N, Cousins AB. **2020**. C_4 grasses adapted to low precipitation habitats show traits related to greater mesophyll conductance and lower leaf hydraulic conductance. *Plant, Cell & Environment* **43**: 1897–1910.

Peters JMR, López R, Nolf M, Hutley LB, Wardlaw T, Cernusak LA, Choat B. **2021**. Living on the edge: A continental-scale assessment of forest vulnerability to drought. *Global Change Biology* **27**: 3620–3641.

Pfautsch S, Harbusch M, Wesolowski A, Smith R, Macfarlane C, Tjoelker MG, Reich PB, Adams MA. **2016**. Climate determines vascular traits in the ecologically diverse genus *Eucalyptus* (F Lloret, Ed.). *Ecology Letters* **19**: 240–248.

Pittermann J, Sperry JS. **2006**. Analysis of Freeze-Thaw Embolism in Conifers. The Interaction between Cavitation Pressure and Tracheid Size. *Plant Physiology* **140**: 374–382.

Powers JS, Vargas G. G, Brodribb TJ, Schwartz NB, Pérez-Aviles D, Smith-Martin CM, Becknell JM, Aureli F, Blanco R, Calderón-Morales E, *et al.* 2020. A catastrophic tropical drought kills hydraulically vulnerable tree species. *Global Change Biology* **26**: 3122–3133.

Salleo S, Nardini A, Pitt F, Gullo MAL. **2000**. Xylem cavitation and hydraulic control of stomatal conductance in Laurel (*Laurus nobilis* L.). *Plant, Cell & Environment* **23**: 71–79.

Savi T, Marin M, Luglio J, Petruzzellis F, Mayr S, Nardini A. **2016**. Leaf hydraulic vulnerability protects stem functionality under drought stress in Salvia officinalis. *Functional Plant Biology* **43**: 370.

Schwinning S, Lortie CJ, Esque TC, DeFalco LA. **2022**. What common-garden experiments tell us about climate responses in plants. *Journal of Ecology* **110**: 986–996.

Scoffoni C, Albuquerque C, Brodersen CR, Townes SV, John GP, Bartlett MK, Buckley TN, McElrone AJ, Sack L. **2017**. Outside-Xylem Vulnerability, Not Xylem Embolism, Controls Leaf Hydraulic Decline during Dehydration. *Plant Physiology* **173**: 1197–1210.

Scoffoni C, Albuquerque C, Buckley TN, Sack L. **2023**. The dynamic multi-functionality of leaf water transport outside the xylem. *New Phytologist* **239**: 2099–2107.

Scoffoni C, Chatelet DS, Pasquet-kok J, Rawls M, Donoghue MJ, Edwards EJ, Sack L. **2016**. Hydraulic basis for the evolution of photosynthetic productivity. *Nature Plants* **2**: 16072.

Skelton RP, Brodribb TJ, McAdam SAM, Mitchell PJ. **2017**. Gas exchange recovery following natural drought is rapid unless limited by loss of leaf hydraulic conductance: evidence from an evergreen woodland. *New Phytologist* **215**: 1399–1412.

Skelton RP, West AG, Dawson TE. **2015**. Predicting plant vulnerability to drought in biodiverse regions using functional traits. *Proceedings of the National Academy of Sciences* **112**: 5744–5749.

Snyman HA, Ingram LJ, Kirkman KP. **2013**. *Themeda triandra* : a keystone grass species. *African Journal of Range & Forage Science* **30**: 99–125.

Sperry JS. **2000**. Hydraulic constraints on plant gas exchange. *Agricultural and Forest Meteorology* **104**: 13–23.

Sperry JS, Hacke UG, Pittermann J. **2006**. Size and function in conifer tracheids and angiosperm vessels. *American Journal of Botany* **93**: 1490–1500.

Taylor SH, Ripley BS, Woodward FI, Osborne CP. **2011**. Drought limitation of photosynthesis differs between C_3 and C_4 grass species in a comparative experiment. *Plant, Cell & Environment* **34**: 65–75.

Thonglim A, Delzon S, Larter M, Karami O, Rahimi A, Offringa R, Keurentjes JJB, Balazadeh S, Smets E, Lens F. **2021**. Intervessel pit membrane thickness best explains variation in embolism resistance amongst stems of *Arabidopsis thaliana* accessions. *Annals of Botany* **128**: 171–182.

Tombesi S, Nardini A, Farinelli D, Palliotti A. **2014**. Relationships between stomatal behavior, xylem vulnerability to cavitation and leaf water relations in two cultivars of *Vitis vinifera*. *Physiologia Plantarum* **152**: 453–464.

Torres-Ruiz JM, Kremer A, Carins Murphy MR, Brodribb T, Lamarque LJ, Truffaut L, Bonne F, Ducousso A, Delzon S. **2019**. Genetic differentiation in functional traits among European sessile oak populations (J-P Schnitzler, Ed.). *Tree Physiology* **39**: 1736–1749.

Trueba S, Pouteau R, Lens F, Feild TS, Isnard S, Olson ME, Delzon S. **2017**. Vulnerability to xylem embolism as a major correlate of the environmental distribution of rain forest species on a tropical island. *Plant, Cell & Environment* **40**: 277–289.

Tyree MT, Sperry JS. **1988**. Do Woody Plants Operate Near the Point of Catastrophic Xylem Dysfunction Caused by Dynamic Water Stress? 1: Answers from a Model. *Plant Physiology* **88**: 574–580.

VanderWeide BL, Hartnett DC, Carter DL. **2014**. Belowground bud banks of tallgrass prairie are insensitive to multi-year, growing-season drought. *Ecosphere* **5**: art103.

Volaire F, Lens F, Cochard H, Xu H, Chacon-Doria L, Bristiel P, Balachowski J, Rowe N, Violle C, Picon-Cochard C. **2018**. Embolism and mechanical resistances play a key role in dehydration tolerance of a perennial grass Dactylis glomerata L. *Annals of Botany* **122**: 325–336.

Volaire F, Seddaiu G, Ledda L, Lelievre F. **2009**. Water deficit and induction of summer dormancy in perennial Mediterranean grasses. *Annals of Botany* **103**: 1337–1346.

Wortemann R, Herbette S, Barigah TS, Fumanal B, Alia R, Ducousso A, Gomory D, Roeckel-Drevet P, Cochard H. **2011**. Genotypic variability and phenotypic plasticity of cavitation resistance in Fagus sylvatica L. across Europe. *Tree Physiology* **31**: 1175–1182.

Xiong D, Douthe C, Flexas J. **2018**. Differential coordination of stomatal conductance, mesophyll conductance, and leaf hydraulic conductance in response to changing light across species. *Plant, Cell & Environment* **41**: 436–450.

Yao G, Nie Z, Turner NC, Li F, Gao T, Fang X, Scoffoni C. **2021**. Combined high leaf hydraulic safety and efficiency provides drought tolerance in *Caragana* species adapted to low mean annual precipitation. *New Phytologist* **229**: 230–244.

Zanne AE, Westoby M, Falster DS, Ackerly DD, Loarie SR, Arnold SEJ, Coomes DA. **2010**. Angiosperm wood structure: Global patterns in vessel anatomy and their relation to wood density and potential conductivity. *American Journal of Botany* **97**: 207–215.

Zhang Q, Shen H, Peng L, Tao Y, Zhou X, Yin B, Fan Z, Zhang J. **2024**. Intraspecific Variability of Xylem Hydraulic Traits of Calligonum mongolicum Growing in the Desert of Northern Xinjiang, China. *Plants* **13**: 3005.

Zhou H, Akçay E, Edwards E, Helliker B. **2020**. The legacy of C_4 evolution in the hydraulics of C_3 and C_4 grasses.

Zwicke M, Picon-Cochard C, Morvan-Bertrand A, Prud'homme M-P, Volaire F. **2015**. What functional strategies drive drought survival and recovery of perennial species from upland grassland? *Annals of Botany* **116**: 1001–1015.